IEEE Access
Multidisciplinary ⋮ Rapid Review ⋮ Open Access Journal

Received January 26, 2020, accepted March 8, 2020, date of current version March 31, 2020.

Digital Object Identifier 10.1109/ACCESS.2020.2982275

Plasmonic FET Terahertz Spectrometer

XUEQING LIU[1], TROND YTTERDAL[2], (Senior Member, IEEE), AND MICHAEL SHUR[1,3], (Life Fellow, IEEE)

[1]Department of Electrical, Computer, and Systems Engineering, Rensselaer Polytechnic Institute, Troy, NY 12180, USA
[2]Department of Electronic Systems, Norwegian University of Science and Technology, 7491 Trondheim, Norway
[3]Electronics of the Future, Inc., Vienna, VA 22181, USA

Corresponding author: Michael Shur (shurm13@gmail.com)

This work was supported in part by the U.S. Army Research Laboratory Cooperative Research Agreement at Rensselaer Polytechnic Institute (RPI) (Project Monitor Dr. Meredith Reed), and in part by the U.S. Air Force Office of Scientific Research (AFOSR) (Project Monitor Dr. Kenneth Goretta).

ABSTRACT We show that Si MOSFETs, AlGaN/GaN HEMTs, AlGaAs/InGaAs HEMTs, and p-diamond FETs with feature sizes ranging from 20 nm to 130 nm could operate at room temperature as THz spectrometers in the frequency range from 110 GHz to 9.2 THz with different subranges corresponding to the transistors with different features sizes and tunable by the gate bias. The spectrometer uses a symmetrical FET with interchangeable source and drain with the rectified THz voltage between the source and drain being proportional to the sine of the phase shift between the voltages induced by the THz signal between gate-to-drain and gate-to-source. This phase difference could be created by using different antennas for the source-to-gate and drain-to gate contacts or by using a delay line introducing a phase shift or even by manipulating the impinging angle of the two antennas. The spectrometers are simulated using the multi-segment unified charge control model implemented in SPICE and ADS and accounting for the electron inertia effect and the distributed channel resistances, capacitances and Drude inductances.

INDEX TERMS Terahertz, FET, spectrometer, SPICE, unified charge control model.

I. INTRODUCTION

Terahertz (THz) technology applications ranging from spectroscopy and imaging, non-destructive testing, quality control, and communications [1]–[10] require sensitive detectors of THz and sub-THz radiation. Plasmonic field effect transistors (also called TeraFETs) have demonstrated excellent performance as THz and sub-THz detectors [11]–[13] and potential for THz generation [14], [15]. A recent proposal is to use TeraFETs as spectrometers and interferometers of THz and sub-THz radiation based on the frequency-dependent THz signal rectification resulting from the phase difference in the THz voltages induced between the source-gate and drain-gate contacts of a single FET detector [16]. The qualitative analytical theory presented in [16] showed that the TeraFET spectrometer response varies from positive to negative with the gate bias. The gate voltage, at which the response is zero, depends on the frequency of the impinging THz signal that could be accurately determined. The strength of the response is proportional to $\sin\theta$, where θ is the phase difference between the signals coupled to the gate-to-source and gate-to-drain contacts.

In this work, we simulate Si MOSFETs with feature sizes ranging from 20 nm to 130 nm and determine the TeraFET spectrometer operating ranges as functions of the device feature size. Our results show that such Si-based THz spectrometers could operate in the frequency range from 110 GHz to 9.2 THz. Using Si TeraFET that are fabricated using a standard Si VLSI technology opens up unique capabilities for cost-effective THz electronics technology and an avenue for a quick commercialization. Our results show that other materials systems might have advantages compared to silicon for the THz spectrometer applications, especially at higher frequency. However, the commercialization for these materials systems presents a greater challenge, especially for p-diamond promising the highest performance in the 240 to 320 GHz range, which is of most interest for Beyond 5G applications but probably further in the future in terms of the commercialization potential.

For the simulations, we use the unified charge control THz SPICE model for plasmonic field effect transistors implemented in Verilog-A [17], [18]. It has been validated for FETs in various feature sizes and different material

The associate editor coordinating the review of this manuscript and approving it for publication was Yue Zhang.

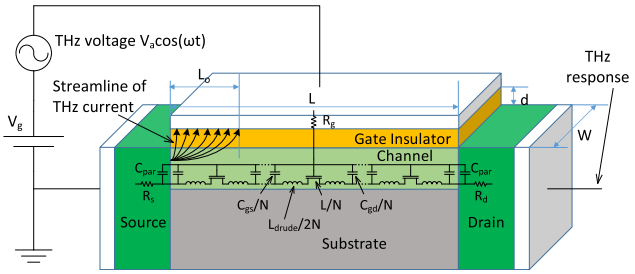

FIGURE 1. Plasmonic FET under THz radiation modeled with multiple segments in the channel accounting for the THz current distribution.

systems including 20 nm FDSOI MOSFETs and 130 nm AlGaAs/InGaAs pHEMTs [17], [18].

The THz spectrometer simulations using the SPICE model show that the signal detected as the drain-to-source voltage at the modulation frequency of the impinging THz radiation drops to zero at the frequency that is tunable by the gate voltage and establish the spectrometer frequency detection ranges that are functions of the gate length and the gate-source voltage. Our preliminary analysis show that the process variations could be adjusted during spectrometer calibration by relating the cross-over frequencies to the gate bias. A more detailed analysis of the process variation effects will be presented in the following sections.

II. THz SPICE MODEL

The response of TeraFETs in the THz frequency range is the rectified drain-to-source voltage appearing due to the rectification of the decayed or resonant plasma waves in the FET channel [19]–[21]. Fig. 1 illustrates the operating principle of a standard TeraFET THz detector with the transmission line in the device channel and the gate-to-channel current streamlines due to the impinging THz radiation. The impinging THz radiation couples to the FET via antennas connected to the gate-to-source and/or also to the gate-to-drain circuits or even just to the interconnects and contact pads. The excitations of the electron density – plasma waves – excited by the voltages at the THz frequencies due to the impinging radiation are rectified due to the nonlinear electron transport in the FET channel. The induced voltage across the FET channel is a DC drain-to-source voltage or (more practical) lower frequency voltage modulated due to the modulation of the impinging THz signal and measured by a lock-in amplifier to increase the signal-to-noise ratio. For $\omega\tau \ll 1$, where ω is the THz frequency and $\tau = m\mu/q$ is the momentum relaxation time, μ is the mobility, m is the effective mass, and q is the electronic charge, the plasma waves are overdamped. For $\omega\tau \gg 1$, the plasma waves are resonant [22]. For the standard TeraFET THz detector, the most efficient regime is when the THz signal is only coupled to the gate-to-source contacts as shown in Fig. 1. The analytical THz detector theory was first derived for the above threshold regime [20] and was then generalized to include the subthreshold regime and the parasitic resistances capacitances [17].

Fig. 1 also shows the nonlinear transmission line representing the equivalent circuit in the transistor channel. In addition to the capacitances representing the gate-to-channel coupling and resistances accounting for the electron scattering in the device channel this improved equivalent circuit includes Drude inductances accounting for the electron inertia and important or even dominant at high frequencies [23]. Fig. 1 also schematically shows the THz current crowding near the gate edge due to low distributive capacitive impedance at high frequencies.

The unified charge control model (UCCM) yields the equations for the intrinsic FET capacitances C_{gs} and C_{gd} [18]. The SPICE model accounts for the extrinsic components including the parasitic capacitances C_{par} and the series resistances R_g, R_s and R_d. The Drude inductance $L_{drude} = \tau R_{ch}$, where R_{ch} is the channel resistance, accounts for the electron inertia [24] and, therefore, allows to describe the plasmonic resonances. To account for the THz current crowding, the channel is split into segments. The required number of segments $N \geq 3L/L_o$, where L is the channel length and $L_o = \sqrt{\mu V_{gt}/(2\pi f)}$, where f is the THz radiation frequency, $V_{gt} = V_{gs} - V_{TH}$ is the gate voltage swing, V_{TH} is the threshold voltage [25]. L_o represents the characteristic scale of the voltage variation along the FET channel, which must be accounted at frequencies such that $L_o < L$ requiring the channel segmentation in the FET model. Fig. 2 shows the minimum required number of the segments needed for different material systems as a function of the THz frequency and FET channel length.

Fig. 3 compares the simulated I-V characteristic with the measured I-Vs for AlGaAs/InGaAs pHEMTs with 130 nm gate length and 18 μm gate width fabricated by Qorvo Inc. Fig. 4 compares the simulated I-V characteristics with the Sentaurus TCAD simulation results for a 20 nm FDSOI NMOS ($W = 1\,\mu$m and $L = 17$ nm). These comparisons validate our multi-segment UCCM SPICE/ADS model for different material systems.

III. ANALYTICAL MODEL AND SPICE SIMULATION RESULTS FOR THz SPECTROMETER

Fig. 5 (a) shows the schematic of the spectrometer using a single plasmonic FET [16]. In the spectrometer regime of operation, the symmetry between the source and drain is broken by the phase shift θ of the THz voltages applied between the gate-source and gate-drain terminals.

In the above threshold regime, the rectified voltage across the FET channel due to the impinging THz radiation is given by [16]

$$V = \frac{\beta\omega V_a^2 \sin\theta}{4V_{gt}|\sin(kL)|^2\sqrt{\omega^2+\gamma^2}}. \quad (1)$$

Here L is the channel length, V_a is the THz voltage magnitude (the same between gate-source and gate-drain), $\omega = 2\pi f$, $\gamma = 1/\tau$, $k = (\Omega + i\Gamma)/s$ is the plasma wave vector, $\Omega = \sqrt{\sqrt{\omega^4+\omega^2\gamma^2}/2 + \omega^2/2}$, $\Gamma = \sqrt{\sqrt{\omega^4+\omega^2\gamma^2}/2 - \omega^2/2}$,

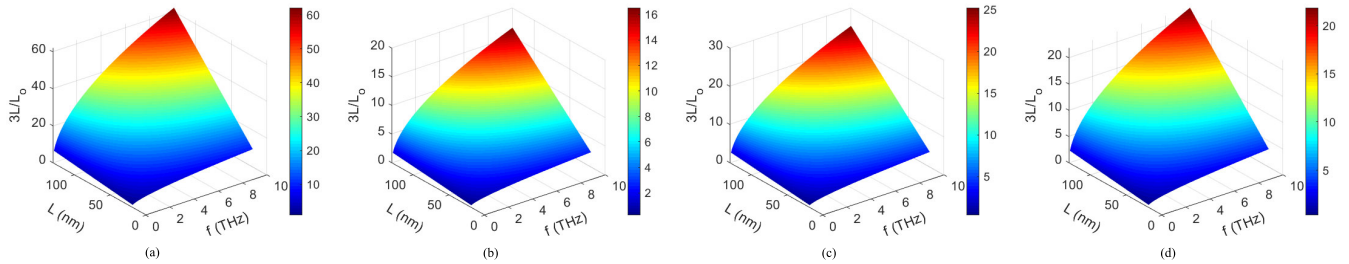

FIGURE 2. Minimum number of segments needed for the multi-segment model: (a) Si ($V_{gt} = 0.11$ V, $\mu = 0.05\,\mathrm{m^2/Vs}$), (b) InGaAs ($V_{gt} = 0.1$ V, $\mu = 0.35\,\mathrm{m^2/Vs}$), (c) GaN ($V_{gt} = 0.1$ V, $\mu = 0.15\,\mathrm{m^2/Vs}$), (d) p-diamond ($V_{gt} = 0.1$ V, $\mu = 0.2\,\mathrm{m^2/Vs}$).

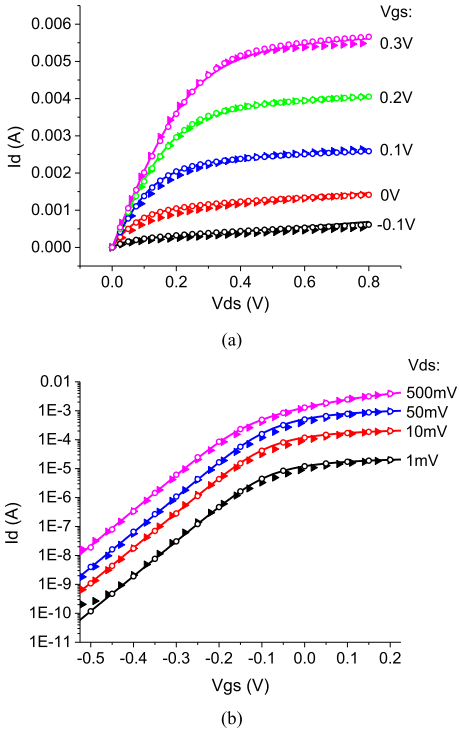

FIGURE 3. Comparison of the simulated I-Vs for the one segment SPICE model (lines) and the multi-segment model (circles) with the measured I-Vs (triangles) for AlGaAs/InGaAs pHEMTs.

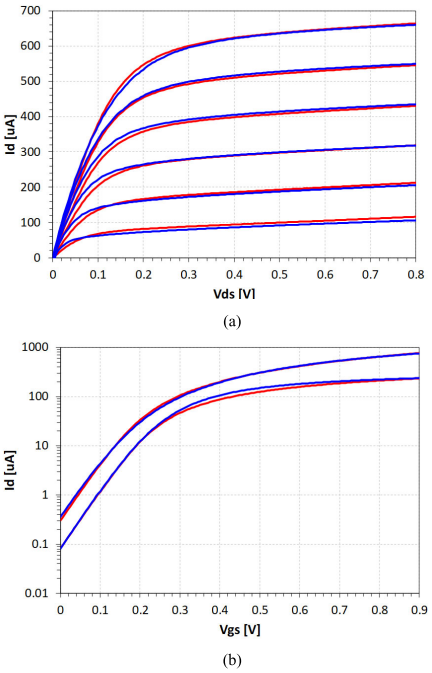

FIGURE 4. Comparison of the simulated I-Vs for the one segment SPICE model (red) with fitted to TCAD simulation results (blue) for the 20 nm FDSOI NMOS ($W = 1\,\mu$m and $L = 17$ nm): (a) output characteristics ($V_{gs} = 0.8$ V for the top curve and step is −0.1V) and (b) transfer characteristics ($V_{ds} = 0.6$ V for the top curve and $V_{ds} = 50$ mV for the bottom curve).

$\beta = 8\sinh(\Gamma L/s)\sin(\Omega L/s)$, s is the plasma wave velocity.

Any one of the steady-state analysis types in the circuit simulator (SPICE or ADS) yields the spectrometer response for the THz spectrometer shown in Fig. 5 (b), where an ideal DC block is used into the equivalent circuit for the extraction of the DC response at the source and drain terminals. However, for a more accurate estimation of the response magnitude, the voltage sources accounting for the impinging THz radiation have to be substituted by more detailed receiving antenna equivalent circuits. $V_a = 10\,\mathrm{mV}$ and $\theta = 90°$ are assumed for the THz signals and 50 segments are used for the SPICE model. Fig. 6 compares the rectified drain-to-source voltage as a function of f for Si, AlGaAs/InGaAs, AlGaN/GaN and p-diamond FETs between the analytical model and the ADS simulation. The difference is due to the analytical model not accounting for the capacitive coupling between the drain, source, and gate. The analytical theory is not valid below threshold and does not account for parasitics that are important or even dominant for ultra-short channel FETs. Our compact multi-segment THz model resolves these issues and is suitable for the spectrometer design. Fig. 7 shows the effect of series resistance on the simulated spectrometer response. It could be seen that InGaAs based HFET is much more sensitive to the series resistance than other FETs especially Si MOS.

Fig. 8 shows the effect of the gate bias on the THz spectrometer response. It could be seen that with the increase of the gate bias, the lowest cross-over frequency f_{co} increases, while the response magnitude decreases. Fig. 9 shows the lowest cross-over frequency f_{co} for different gate biases. Different FETs with different feature sizes could operate as the THz spectrometer in different frequency bands. For example, the subrange for the 20 nm Si MOS spectrometer

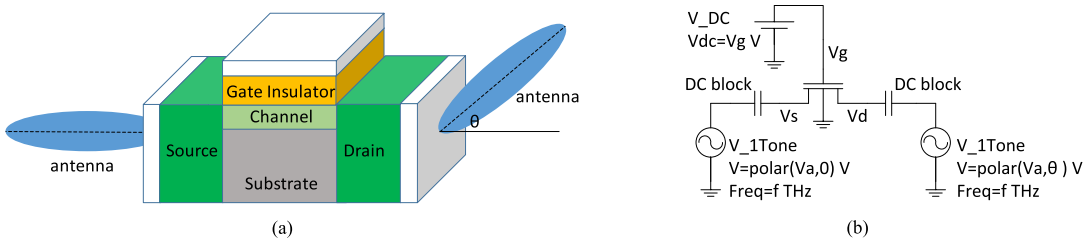

FIGURE 5. Schematics of operating a single plasmonic FET as a spectrometer [16] (a) and the THz spectrometer simulation (b).

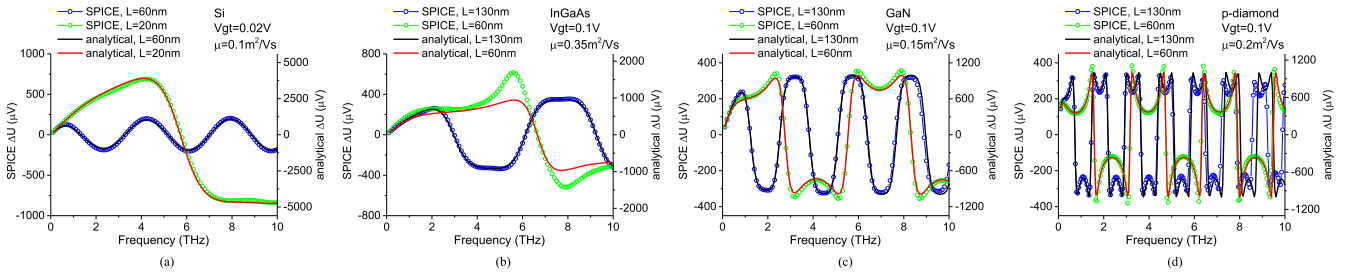

FIGURE 6. Spectrometer response as a function of frequency for (a) Si ($m = 0.19$), (b) InGaAs ($m = 0.041$), (c) GaN ($m = 0.24$), and (d) p-diamond ($m = 0.74$) without series resistance ($R_g = R_s = R_d = 0\,\Omega$).

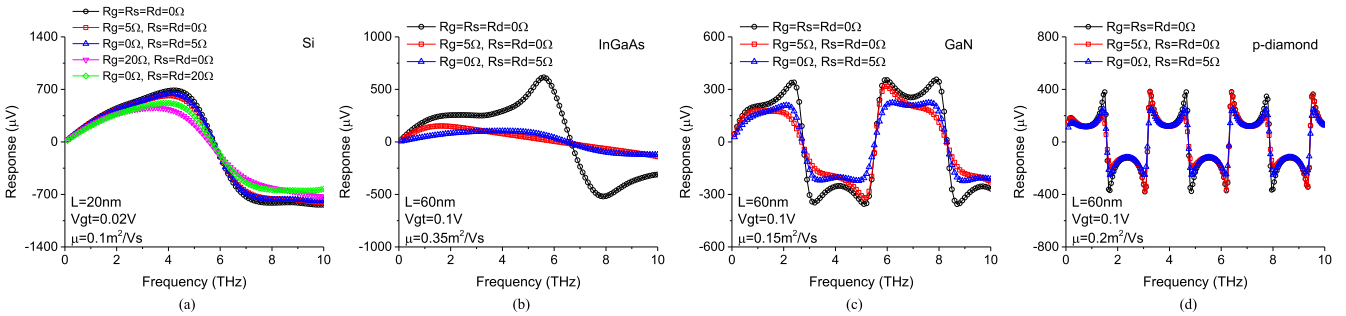

FIGURE 7. Effect of series resistance on the simulated spectrometer response as a function of frequency for (a) Si, (b) InGaAs, (c) GaN, and (d) p-diamond.

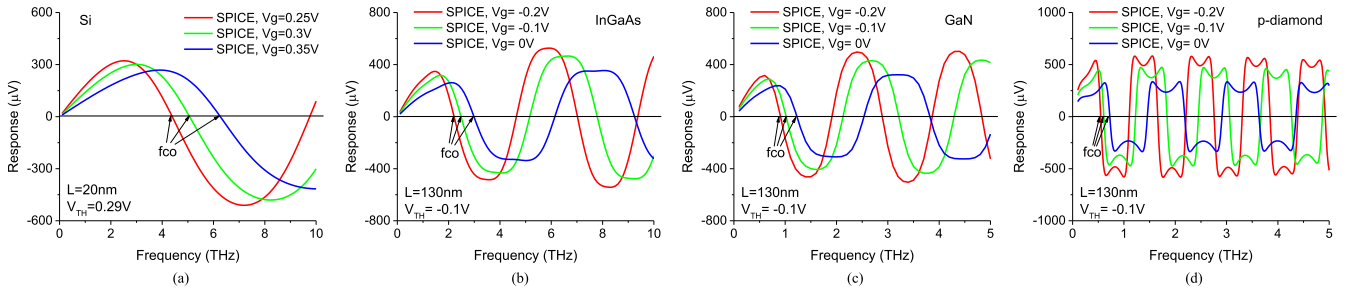

FIGURE 8. Simulated THz spectrometer response as a function of frequency at different gate biases for (a) Si ($\mu = 0.05\,m^2/Vs$), (b) InGaAs ($\mu = 0.35\,m^2/Vs$), (c) GaN ($\mu = 0.15\,m^2/Vs$), (d) p-diamond ($\mu = 0.2\,m^2/Vs$) without series resistance ($R_g = R_s = R_d = 0\,\Omega$).

is from 4.1 THz to 9.2 THz. For Si MOS with feature sizes from 20 nm to 130 nm it is possible to cover the continuous THz band from 110 GHz to 9.2 THz, while the frequency bands covered for InGaAs, GaN and p-diamond FETs with feature sizes from 60 nm to 130 nm are from 2.2 THz to 8 THz, from 0.9 THz to 3.3 THz, and from 0.5 THz to 1.9 THz, respectively. Fig. 10 shows the comparison of the f_{co} range in different material systems with different feature sizes using the THz SPICE model. It could be seen that FETs with shorter channels should be selected as the spectrometers applied at higher THz frequencies. With the same feature size, InGaAs FETs are more suitable for spectrometers operating at high THz frequencies than Si FETs.

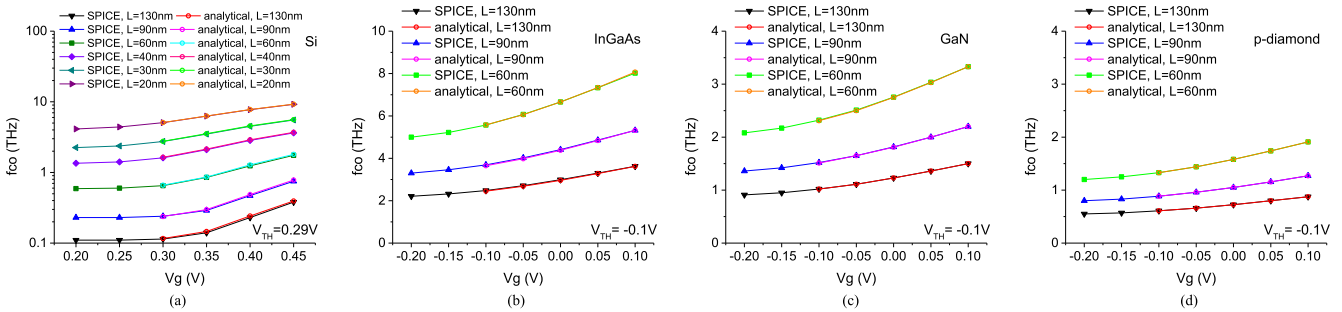

FIGURE 9. **Extracted cross-over frequency as a function of gate bias for the SPICE model compared with the analytical results for (a) Si ($\mu = 0.05\,m^2/Vs$), (b) InGaAs ($\mu = 0.35\,m^2/Vs$), (c) GaN ($\mu = 0.15\,m^2/Vs$), (d) p-diamond ($\mu = 0.2\,m^2/Vs$) without series resistance ($R_g = R_s = R_d = 0\,\Omega$).**

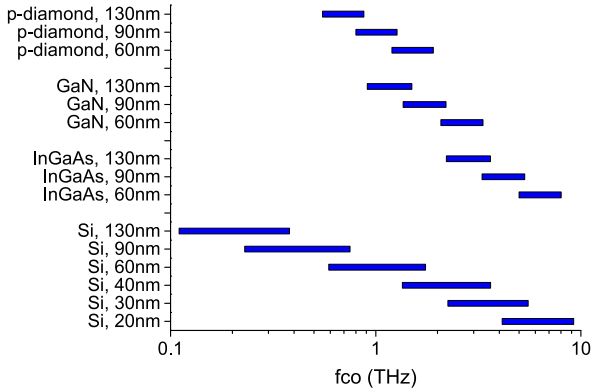

FIGURE 10. **Comparison of the cross-over frequency range in different material systems with different feature sizes using the THz SPICE model.**

IV. CONCLUSION

Using our compact multi-segment THz SPICE/ADS model accounting for the electron inertia and the distributed channel impedance, we simulated THz spectrometers using Si, InGaAs, GaN, and p-diamond FETs. Our results show that using the phase shift in the THz radiation coupling to the gate-to-source and gate-to-drain contacts, Si MOSFETs with feature sizes from 20 nm to 130 nm could operate as THz spectrometers in the 110 GHz to 9.2 THz frequency range, while InGaAs, GaN and p-diamond FETs with feature sizes from 60 nm to 130 nm could operate as the THz spectrometers in the 2.2 THz to 8 THz, 0.9 THz to 3.3 THz, and 0.5 THz to 1.9 THz frequency ranges, respectively. The spectrometers are tunable by the gate bias. This technology should enable novel THz components and systems for THz interferometry, imaging, and communications, including communications in Beyond 5G 240 GHz to 300 GHz range.

ACKNOWLEDGMENT

The authors are grateful to Dr. V. Kachorovskii for useful discussions.

REFERENCES

[1] D. M. Mittleman, "Twenty years of terahertz imaging," *Opt. Express*, vol. 26, no. 8, pp. 9417–9431, Apr. 2018.

[2] J. A. Zeitler, T. Rades, and P. F. Taday, "Pharmaceutical and security applications of terahertz spectroscopy," in *Terahertz Spectroscopy: Principles and Applications*, S. L. Dexheimer, Ed. 1st ed. Boca Raton, FL, USA: CRC Press, 2017, pp. 323–348.

[3] Q. Sun, Y. He, K. Liu, S. Fan, E. P. Parrott, and E. Pickwell-MacPherson, "Recent advances in terahertz technology for biomedical applications," *Quantum Imag. Med. Surg.*, vol. 7, no. 3, pp. 345–355, Jun. 2017.

[4] S. Nellen, B. Globisch, R. B. Kohlhaas, L. Liebermeister, and M. Schell, "Recent progress of continuous-wave terahertz systems for spectroscopy, non-destructive testing, and telecommunication," *Proc. SPIE, Terahertz, RF, Millim., Submillimeter-Wave Technol. Appl. XI*, vol. 10531, Feb. 2018, Art. no. 105310C.

[5] S. Zhong, "Progress in terahertz nondestructive testing: A review," *Frontiers Mech. Eng.*, vol. 14, no. 3, pp. 273–281, Sep. 2019.

[6] K. Ahi, S. Shahbazmohamadi, and N. Asadizanjani, "Quality control and authentication of packaged integrated circuits using enhanced-spatial-resolution terahertz time-domain spectroscopy and imaging," *Opt. Lasers Eng.*, vol. 104, pp. 274–284, May 2018.

[7] L. A. Hejri, P. Hajeb, P. Ara, and R. J. Ehsani, "A comprehensive review on food applications of terahertz spectroscopy and imaging," *Comprehensive Rev. Food Sci. Food Saf.*, vol. 18, no. 5, pp. 1563–1621, Sep. 2019.

[8] M. Shur, "Plasmonic detectors and sources for THz communication and sensing," *Proc. SPIE, Micro-Nanotechnol. Sensors, Syst., Appl. X*, vol. 10639, May 2018, Art. no. 1063929.

[9] M. Shur, "TeraFETs for terahertz communications," *Photon. Newslett.*, vol. 33, no. 3, pp. 4–7, Jun. 2019.

[10] S. L. Rumyantsev, A. Muraviev, S. Rudin, G. Rupper, M. Reed, J. Suarez, and M. Shur, "Terahertz beam testing of millimeter wave monolithic integrated circuits," *IEEE Sensors J.*, vol. 17, no. 17, pp. 5487–5491, Jul. 2017.

[11] W. Knap, Y. Deng, S. Rumyantsev, and M. S. Shur, "Resonant detection of subterahertz and terahertz radiation by plasma waves in submicron field-effect transistors," *Appl. Phys. Lett.*, vol. 81, no. 24, pp. 4637–4639, Dec. 2002.

[12] A. V. Antonov, V. I. Gavrilenko, E. V. Demidov, S. V. Morozov, A. A. Dubinov, J. Lusakowski, W. Knap, N. Dyakonova, E. Kaminska, A. Piotrowska, K. Golaszewska, and M. S. Shur, "Electron transport and terahertz radiation detection in submicrometer-sized GaAs/AlGaAs field-effect transistors with two-dimensional electron gas," *Phys. Solid State*, vol. 46, no. 1, pp. 146–149, Jan. 2004.

[13] F. Teppe, W. Knap, D. Veksler, M. S. Shur, A. P. Dmitriev, V. Y. Kachorovskii, and S. Rumyantsev, "Room-temperature plasma waves resonant detection of sub-terahertz radiation by nanometer field-effect transistor," *Appl. Phys. Lett.*, vol. 87, no. 5, Aug. 2005, Art. no. 052107.

[14] W. Knap, J. Lusakowski, T. Parenty, S. Bollaert, A. Cappy, V. V. Popov, and M. S. Shur, "Terahertz emission by plasma waves in 60 nm gate high electron mobility transistors," *Appl. Phys. Lett.*, vol. 84, no. 13, pp. 2331–2333, Mar. 2004.

[15] D. Yavorskiy, K. Karpierz, P. Kopyt, M. Grynberg, and J. Łusakowski, "Sub-terahertz emission from field-effect transistors," *Acta Phys. Polonica A*, vol. 132, no. 2, pp. 335–337, Aug. 2017.

[16] I. V. Gorbenko, V. Y. Kachorovskii, and M. Shur, "Terahertz plasmonic detector controlled by phase asymmetry," *Opt. Express*, vol. 27, no. 4, pp. 4004–4013, Feb. 2019.

[17] X. Liu, K. Dovidenko, J. Park, T. Ytterdal, and M. S. Shur, "Compact terahertz SPICE model: Effects of drude inductance and leakage," *IEEE Trans. Electron Devices*, vol. 65, no. 12, pp. 5350–5356, Dec. 2018.
[18] K. Lee, M. Shur, T. Fjeldly, and T. Ytterdal, *Semiconductor Device Modeling for VLSI*. Princeton, NJ, USA: Prentice-Hall, 1993, pp. 441–478.
[19] M. Dyakonov and M. Shur, "Shallow water analogy for a ballistic field effect transistor: New mechanism of plasma wave generation by DC current," *Phys. Rev. Lett.*, vol. 71, no. 15, pp. 2465–2468, Oct. 1993.
[20] M. Dyakonov and M. Shur, "Detection, mixing, and frequency multiplication of terahertz radiation by two-dimensional electronic fluid," *IEEE Trans. Electron Devices*, vol. 43, no. 3, pp. 380–387, Mar. 1996.
[21] M. I. Dyakonov and M. S. Shur, "Plasma wave electronics: Novel terahertz devices using two dimensional electron fluid," *IEEE Trans. Electron Devices*, vol. 43, no. 10, pp. 1640–1645, Oct. 1996.
[22] W. Knap, "Field effect transistors for terahertz detection: Physics and first imaging applications," *J. Infr. Millim. THz Waves*, vol. 30, no. 12, pp. 1319–1337, Dec. 2009.
[23] X. Liu, T. Ytterdal, V. Y. Kachorovskii, and M. S. Shur, "Compact terahertz SPICE/ADS model," *IEEE Trans. Electron Devices*, vol. 66, no. 6, pp. 2496–2501, Jun. 2019.
[24] M. Shur, "Plasma wave terahertz electronics," *Electron. Lett.*, vol. 46, no. 26, pp. 18–21, Dec. 2010.
[25] W. Knap, "Recent results on broadband nanotransistor based Thz detectors," in *Proc. THz Secur. Appl.*, Mar. 2014, pp. 189–209.

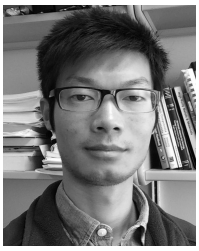

XUEQING LIU received the B.E. and M.E. degrees from the Huazhong University of Science and Technology, Wuhan, China, in 2009 and 2012, respectively, and the Ph.D. degree from Rensselaer Polytechnic Institute, Troy, NY, USA, in 2019. He is currently a Postdoctoral Research Associate with Rensselaer Polytechnic Institute. His current research interest includes modeling and simulation of semiconductor devices.

TROND YTTERDAL (Senior Member, IEEE) received the M.Sc. and Ph.D. degrees in electrical engineering from the Norwegian Institute of Technology, in 1990 and 1995, respectively.

He was employed as a Research Associate at the Department of Electrical Engineering, University of Virginia, from 1995 to 1996, and a Research Scientist at the Electrical, Computer and Systems Engineering Department, Rensselaer Polytechnic Institute, Troy, NY, USA, from 1996 to 1997. From 1997 to 2001, he worked as a Senior ASIC Designer at Nordic Semiconductor, Trondheim, Norway. Since 2001, he has been with the Faculty of the Norwegian University of Science and Technology (NTNU), where he is currently a Professor with the Department of Electronics and Telecommunications. He has authored or coauthored more than 200 scientific articles in international journals and conference proceedings. He is the coauthor of *Semiconductor Device Modeling for VLSI* (Prentice Hall, 1993), *Introduction to Device Modeling and Circuit Simulation* (Wiley, 1998), and *Device Modeling for Analog and RF CMOS Circuit Design* (Wiley, 2003). He has been a contributor to several other books published internationally. He is also a co-developer of the circuit simulator AIM-Spice. His current research interests include design of analog integrated circuits, behavioral modeling and simulation of mixed-signal systems, modeling of nanoscale transistors, and novel device structures for application in circuit simulators.

Dr. Ytterdal is a member of the Norwegian Academy of Technological Sciences.

MICHAEL SHUR (Life Fellow, IEEE) received the M.S. degree in electrical engineering from the St. Petersburg Electrotechnical University and the Ph.D. degree in mathematics and physics and the D.Sc. (Habilitation) degree in mathematics and physics from the A. F. Ioffe Institute of Physics and Technology. He is currently the Patricia W. and C. Sheldon Roberts Professor of solid state electronics with Rensselaer Polytechnic Institute, Troy, NY, USA. He is also the Vice-President and the Chief Technology Officer of Electronics of the Future, Inc. He is a Life Fellow of the American Physical Society and SPIE and a Fellow of OSA, SPIE, IET, AAAS, MRS, WIF, and ECS. He is also a Foreign Member of the Lithuanian Academy of Sciences and a Fellow of the National Academy of Inventors. His awards include the Tibbetts Award for Technology Commercialization, the Honorary Doctorates from the St. Petersburg Technical University and Vilnius University, the IEEE EDS Ebers Award, the Sensors Council Technical Achievement Award, the IEEE Donald Fink Award, the IEEE Kirchmayer Award, the Gold Medal of the Russian Ministry of Education, the van der Ziel Award, the Senior Humboldt Research Award, the Pioneer Award, the RPI Engineering Research Award, several Best Paper Awards, and the Distinguished Lecturer awards from the IEEE EDS, MTT, and the Sensors Council. He is also the Editor-in-Chief of the *International Journal of High Speed Electronics and Systems*.